GPS stations within the stippled area in Figure 1 (that is, SLR velocities are not included in the pole determination). This rotation results in velocities at the NAF of about 25 mm/yr.

As indicated by the residual velocities in Figure 3, deviations from uniform plate motion appear to increase toward the Hellenic arc. The overall pattern suggests crustal extension in the southern Aegean Sea and western Turkey. Crustal extension in this region is generally consistent with independent GPS results from the southern Aegean [Kastens et al., 1993] as well as with earthquake focal mechanisms and geologic structure [McKenzie, 1970; Sengör et al., 1985]. However, the observed stretching rate (10 mm/yr) is considerably less than the overall Anatolian plate motion rate and less than one third of the rates derived from analysis of earthquake data [McKenzie, 1970]. The small magnitude of the residual velocities indicates that this region behaves approximately as a coherent plate (Anatolian plate). The fit between the small circle about this GPS pole and the NAF (Figure 3) provides independent support for this pole location and indicates that the NAF represents the principal boundary between the Anatolian and Eurasian plates. Additional GPS measurements are planned over the next few years, and the much improved space and ground components of the GPS promise to substantially improve our understanding of kinematic and dynamic processes affecting this area of active continental deformation.

Acknowledgments

References

DeMets, C., R.G. Gordon., D. F. Argus, and S. Stein, Current plate motions, Geophys. J. Int., 101, 425, 1990.

Isacks, B., J. Oliver, and L.R. Sykes, Seismology and the new global tectonics, J. Geophys. Res., 73, 5855, 1968.

Jackson, J., and D. McKenzie, The relationship between plate motions and seismic moment tensors, and the rates of active deformation in the Mediterranean and Middle East, Geophys. J. R. Astron. Soc., 93, 45, 1988.

Kastens, K. A., L. E. Gilbert, K. J. Hurst, H. Billiris, D. Paradissis, G. Veis, W. Hoppe, and W. Schluter, GPS evidence for arc-parallel extension along the Hellenic arc, southern Aegean sea, Greece, Geol. Soc. Am. Abstracts with Program, A242, 1993.

McKenzie, D. P., Plate tectonics of the Mediterranean region, Nature, 226, 239, 1970.

Molnar, P., and P. Tapponnier, Cenozoic tectonics of Asia: effects of a continental collision, Science, 189, 419, 1975.

Oral, B., Global Positioning System (GPS) Measurements in Turkey (1988-1992): Kinematics of the Africa-Arabia-Eurasia Plate Collision Zone, Ph.D. thesis, Mass. Inst. of Technol., Cambridge, 344 pp., 1994.

Sengör, A. M. C., N. Görür, and F. Saroglu, Strike-slip faulting and related basin formation in zones of tectonic escape: Turkey as a case study, in Strike-slip Faulting and Basin Formation, edited by K.T. Biddle and N. Christie-Blick, Soc. of Econ. Paleontol. Min. Sec. Publ., p. 37, 1985.

Smith, D. E., R. Kolenkiewicz, J. W. Robbins, P. J. Dunn, and M. H. Torrence, Horizontal crustal motion in the central and eastern Mediterranean inferred from Satellite Laser Ranging measurements, Geophys. Res. Lett., 21, 1979, 1994.

Software Expedites Singular-Spectrum Analysis of Noisy Time Series

Michael D. Dettinger, Michael Ghil, Christopher M. Strong, William Weibel, and Pascal Yiou

A Singular-Spectrum Analysis (SSA) Toolkit is now available for use on computers with X-windows capabilities. The Toolkit provides free, compact, and easy access to SSA and several powerful spectral analysis techniques not readily available in common statistical packages. The current Toolkit, Version 1.1, provides tools for

Michael D. Dettinger, U.S. Geological Survey, Water Resources Division, 5735 Kearney Villa Rd., San Diego, CA 92123; Michael Ghil and Christopher M. Strong, Institute of Geophysics and Planetary Physics, University of California, Los Angeles, CA 90024; William Weibel, Department of Atmospheric Sciences, University of California, Los Angeles; CA 90024; Pascal Yiou, Laboratiore de Modélisation du Climat et de l'Environment, Commissariat à l'Énergie Atomique, Gif-sur-Yvette, France

- breaking down univariate, possibly nonstationary time series into trends, periodic oscillations, other statistically significant components, and noise;
- reconstructing the contributions of selected components to the time series; and
- estimating power spectra of the time series or any of its components by modern spectral methods.

These results are achieved through the SSA, complemented by other spectral estimation tools that include correlograms, the Multi-Taper Method (MTM), and the Maximum Entropy Method (MEM). The philosophy of the Toolkit is that only simultaneous application of several spectral methods provides reliable information on a given time series. The Toolkit is readily extended to new methods but is not expected to become an all-purpose package. General statistical packages, such as SAS or Matlab, are not as easy to use or expand and do not contain the particularly powerful combination of time series analysis tools found in the SSA Toolkit. The Toolkit is being distributed by the Department of Atmospheric Sciences at the University of Cali-
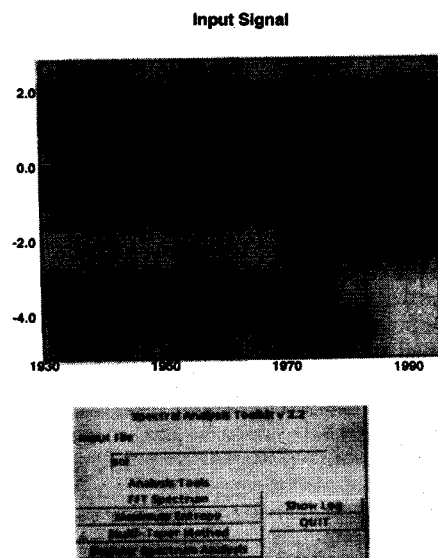
Input Signal

Fig. 1. Toolkit menu and SOI time-series plot, with months from January 1933 on the abscissa and dimensionless SOI values on the ordinate. Original color image appears at back of this volume.
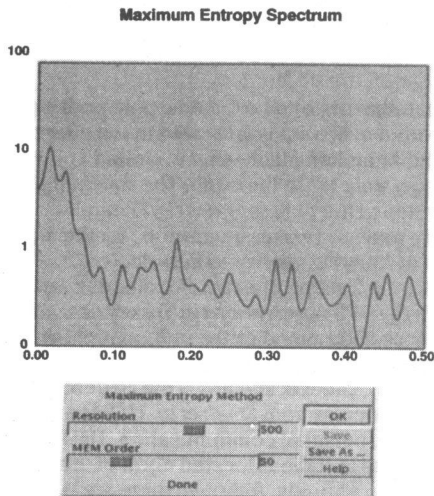
Fig. 2. MEM menu and MEM power spectrum, with frequency in cycles/month on the abscissa and power in months x (dimensionless SOI)^2 on the ordinate. Original color image appears at back of this volume.

fornia, Los Angeles, with contributions from the U.S. Geological Survey and Laboratoire de Modélization du Climat et de l'Environnement.

Toolkit Components

Singular-Spectrum Analysis SSA is designed to extract as much information as possible from short, noisy time series without prior knowledge of the dynamics underlying the series [*Broomhead and King,* 1986; *Vautard and Ghil,* 1989; *Vautard et al.,* 1992]. The method is a form of principal-component (PC) analysis applied to lag-correlation structures of time series. SSA is particularly successful in isolating periodic components and trends. In the Toolkit, it decomposes time series by data-adaptive filters into oscillatory, trending, and noise components; generates statistical significance information on these components; and provides reconstructed components (RCs).

SSA performance is controlled within the Toolkit through the choice of maximum lag (SSA window size), graphical tests of significance level for leading SSA components and a choice of methods for estimating the lag-correlation structure. SSA window size determines its ability to separate oscillations having similar frequencies, with a typical resolution of about [window size]$^{-1}$.

The univariate form of SSA provided by the current Version 1.1 of the Toolkit has seen a number of practical applications. Researchers used it to retrieve periodic oscillations related to El Niño from atmospheric and oceanographic time series [*Rasmusson et al.,* 1990]. *Ghil and Vautard* [1991] retrieved interdecadal temperature variability and global warming trends, and *Penland et al.* [1991] prefiltered angular mo-
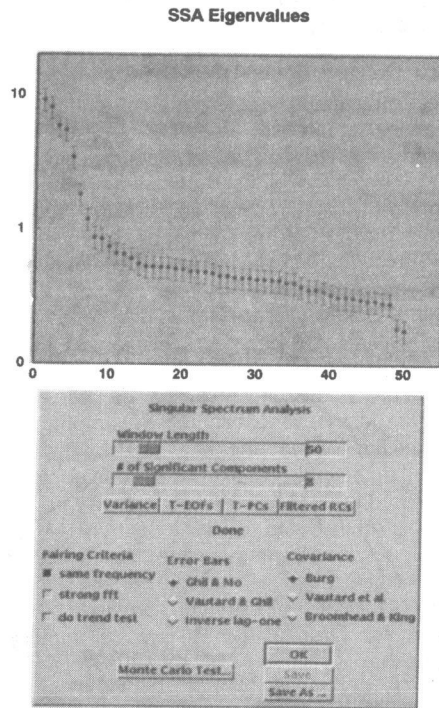

Fig. 3. SSA menu and log-eigenvalue spectrum for the SOI time series, with SSA component number on the abscissa and percentages of total variance on the ordinate. The components are ordered by variance captured. Original color image appears at back of this volume.

mentum time series prior to spectral estimation.

Traditional Fourier-Transform Analysis SSA readily extracts periodic components from nonstationary and noisy time series. To determine the corresponding frequencies, the Toolkit provides several tools for power-spectrum estimation.

Power spectra can be estimated using the windowed-correlogram method of *Marple* [1987]. Correlograms are Fourier transforms of autocorrelations that approximate the power spectrum of the series. They are easily estimated, and the Toolkit provides menu options for choices of windowing functions ("window carpentry" to reduce power leakage within the spectrum) and window widths ("window opening and closing" to control trade-offs between the variance of spectral estimates and the resolution).

Multi-Taper Estimates The Toolkit also provides spectral estimation by the MTM, a non-parametric method developed by *Thomson* [1982]. MTM reduces power leakage and estimation uncertainties by simultaneous application of optimal windowing functions, called tapers, in the time domain. Its significance tests help identify weak spectral peaks and reject high-amplitude bands of noise.

The user controls MTM application by selecting the number of tapers and the frequency bandwidths for which the tapers are optimized. This selection trades off vari-

ance reduction of spectral estimates against reduction of power leakage. The Toolkit automatically highlights spectral peaks that are significant at confidence levels chosen by the user.

Maximum Entropy Estimates The Toolkit also allows spectral estimation by MEM. MEM differs from either the correlogram or MTM by its representation of noisy oscillatory signals as autoregressive (AR) processes, rather than as a sum of sinusoids. Because of this representation, MEM spectra can contain as many sharp spectral peaks, where the spectral density becomes infinite, as the number M of AR terms in the model, and they provide a more data-adaptive description of the overall spectrum.

For high M, MEM yields high-resolution spectra that often include spurious peaks. The Toolkit allows the user to tune the MEM spectrum by choosing M in the AR model. Beyond that, MEM's spurious peaks are eliminated by a combination of approaches: determining which peaks survive reductions in M; comparing MEM spectra to those produced by the correlogram and MTM; and using SSA to prefilter the original series by retaining only the leading RCs—each of which contains only a few spectral peaks [*Penland et al.,* 1991]. The ease of interweaving these various analyses in the Toolkit was a major motivation for its development.

Toolkit Application

To illustrate the flexibility and ease of Toolkit use, we analyze the Southern Oscillation Index (SOI), a climatic indicator of the recurring El Niño condition in the tropical Pacific [*Keppenne and Ghil,* 1992]. SOI is a standardized difference between atmospheric sea level pressures at Darwin, Australia, and Tahiti.

To begin, the SOI series is read into the Toolkit as an ASCII list, producing the curve shown in Figure 1. It has features characteristic of many geophysical time series: considerable irregularity hiding tantalizing suggestions of periodicity. The challenge is to separate the two.

Preliminary Spectral Estimates As a first step, we estimate the power spectrum using MEM. Upon clicking the "Maximum Entropy" button (Figure 1) with the mouse pointer and dragging the "MEM Order" slide (Figure 2) to set the number of AR terms, we calculate an MEM spectrum (Figure 2).

The power spectrum contains two dominant peaks with periods around 52 and 26 months, accompanied by smaller peaks at higher frequencies. The dominant peaks are the low-frequency (LF) and quasi-biennial (QB) components [*Rasmusson et al.,* 1990] of SOI, respectively. At this point (or at any time during the Toolkit session), MTM or correlogram spectra could be used to verify the MEM spectral peaks simply by clicking the appropriate buttons. We find combined
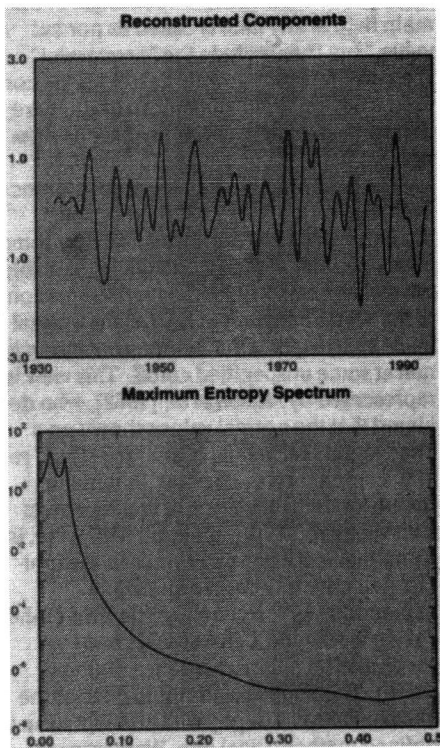
Fig. 4. (a) Reconstruction of SSA components 1-4; same units as in Figure 1b. (b) MEM power spectrum of the SSA-filtered time series shown in (a); same units as in Figure 2. Original color image appears at back of this volume.

application of different spectral methods more enlightening than relying on variance estimates from a single one.

SSA Decomposition SSA can be applied to the data to extract the oscillatory components, to display the variability they represent, or to remove noise prior to renewed spectral estimation. The resulting Toolkit menu and SSA eigenvalue spectrum appear in Figure 3. As in other PC analyses, each SSA eigenvalue is equal to the variance captured by the corresponding component, and structured signals typically rise above the flat tail of the eigenvalue spectrum that represents noise. *Vautard and Ghil* [1989] showed that oscillatory parts of a time series are isolated by pairs of SSA components with nearly equal eigenvalues. The eigenvalue spectrum (Figure 3) shows two leading pairs of nearly equal eigenvalues: 1-2 and 3-4; they are found to correspond, indeed, to oscillations. The Toolkit display includes ad hoc error bars to account for sampling effects on eigenvalue estimation; these bars help the user evaluate breaks in spectral slope between signal and noise and potential pairing of eigenvalues. The Toolkit also offers options for estimating eigenvalue sampling errors by Monte Carlo simulations of either white [*Ghil and Vautard*, 1991; *Vautard et al.*, 1992] or AR [*Allen and Smith*, 1994] noise.

SSA decomposition into oscillations, trends, and noise is achieved in terms of temporal empirical-orthogonal functions (T-EOFs) and temporal PCs (T-PCs), that are recurring temporal patterns and their time-varying amplitudes, respectively. These representations can be examined by clicking the "T-EOFs" or "T-PCs" buttons (Figure 3). In this brief illustration, we jump ahead to reconstruct the leading oscillations by clicking on the "Filtered RCs" button and selecting for reconstruction the first four SSA components. The result is the filtered time series shown in Figure 4a; it captures the main features of the original one in Figure 1, while effectively removing the noisy part. Notice, in Figure 4a, the marked increase in amplitude of the filtered SOI series after 1970, following a lull in the mid-century. Information about the amplitude variations of oscillatory signals, usually lost in standard spectral analyses, is an immediate output from SSA.

Finally, the RC series can be analyzed by any of the spectral estimators provided. The power spectrum of each RC is much simpler than that of the complete time series [*Penland et al.*, 1991; *Vautard et al.*, 1992]. The MEM spectrum for the SSA-filtered series shown in Figure 4b displays an increase in the signal-to-noise ratio from 10 for the unfiltered data (Figure 2) to 108 for the filtered data (Figure 4b). In this example, an initial MEM spectrum (Figure 2) showed peak power at 26 and 52 months. The use of SSA provided data-adaptive filters for the oscillations (Figure 3) without having to search for some nominally optimal band pass filter. The leading oscillatory components were reconstructed (Figure 4a) and passed again through the maximum entropy analysis (Figure 4b). The next step in such an analysis (not shown) is using the Toolkit to quickly explore the sensitivity of results to various MEM orders and SSA window lengths, to confirm the MEM spectrum by application of other spectral estimators [*Vautard et al.*, 1992] or to investigate other SSA components above the noise level in Figure 3.

Toolkit Availability

The SSA Toolkit has a convenient X-windows graphical user interface (GUI) to ensure easy, quick operation. The GUI is based on the Tcl/Tk package [*Ousterhout*, 1994]. Beneath the GUI are several FORTRAN and C programs:

ssa Performs SSA decomposition and selected reconstructions of an input time series.

spectrum Computes windowed correlogram and MEM power spectra.

mtm Computes MTM spectral amplitudes.

carlo Generates Monte Carlo realizations of white or red noise; computes error bars for the SSA eigenvalues based on those realizations.

These numerical programs are functional, without the GUI, on any machine with standard FORTRAN 77 and C compilers. The programs are structured as Unix commands and can be invoked in batch mode by simple scripts. Source codes are provided. New tools in the form of one-pass, argument-driven Unix-style commands can be added directly to the Toolkit, although the creation of new control panels requires some knowledge of Tcl/Tk. The GUI, which displays various time series and spectra to windows, can accommodate different graphics packages. Currently, the Toolkit supports visualization using IDL (a proprietary package by Research Systems, Inc.) or the public domain packages ACE/gr and gnuplot. The graphics packages used to display Toolkit graphs can copy these to postscript files for printing.

Time series are input as ASCII lists. Practical size constraints on Toolkit analyses usually arise from the width of the SSA or correlogram windows or the number of Monte Carlo realizations used to compute error bars, rather than the length of the time series. As a practical matter, window widths should be less than about 300–500, but such limits depend on the size and speed of the computational device—workstation or mainframe—used.

The Toolkit has been ported to DEC, Sun, Silicon Graphics, IBM RS6000, and Data General workstations, and should be transportable to many other computers. Installation of the software requires about 5 Mbytes of storage. A compressed version of the software and documentation can be obtained by Internet users through anonymous ftp at /pub/SSAToolkit.tar.Z on yosemite.atmos.ucla.edu. Users with access to the World-Wide Web can get the Toolkit and supporting software by raising the Web page at http://www.atmos.ucla.edu/ and following the link to the Toolkit. Users without access to ftp can obtain copies for a fee by contacting William Weibel, Department of Atmospheric Sciences, University of California, Los Angeles, 7127 Math Sciences Building, Los Angeles, CA 90024-1565. An Internet mailing list (ssahelp@atmos.ucla.edu) has been instituted to handle questions, suggestions, and bug reports.

The Toolkit is an evolving package designed with room for future additions and enhancements. We encourage feedback on its form and future. Other spectral tools, especially extension to multivariate analysis, are planned for future versions. Further elaboration of the confidence tests for SSA (including that of Allen and Smith (1994)) and Multi-Taper Method, also under consideration, may appear in future versions of the Toolkit. The analytical power and user friendliness of the Toolkit should make geophysical data analysis much more tractable.

References

Allen, M.R., and L. A. Smith, Investigating the origins and significance of low-frequency modes of climate variability, *Geophys. Res. Lett.*, *21*, 883, 1994.
Broomhead, D.S., and G. King, Extracting qualitative dynamics from experimental data, *Physica D*, *20*, 217, 1986.
Ghil, M., and R. Vautard, Interdecadal oscillations and the warming trend in global temperature time series, *Nature, 350*, 324, 1991.
Marple, S.L., *Digital Spectral Analysis, With Applications*, Prentice-Hall, New York, 492 pp., 1987.
Ousterhout, J.K., *Tcl and the Tk Toolkit*, Addison-Wesley, New York, 512 pp., 1994.
Penland, M.C., M. Ghil, and K. Weickmann, Adaptive filtering and maximum entropy spectra with application to changes in atmospheric angular momentum, *J. Geophys. Res., 96*, 22,659, 1991.
Rasmusson, E.M., X. Wang, and C. F. Ropelewski, The biennial component of ENSO variability, *J. Marine Syst., 1*, 71, 1990.
Thomson, D.J., Spectrum estimation and harmonic analysis, *Proc. IEEE, 70*, 1055, 1982.
Vautard, R., and M. Ghil, Singular spectrum analysis in nonlinear dynamics, with applications to paleoclimatic time series, *Physica D, 35*, 395, 1989.
Vautard, R., P. Yiou, and M. Ghil, Singular-spectrum analysis: A toolkit for short, noisy chaotic signals, *Physica D, 58*, 95, 1992.

Scientists Get a Closer Look at Mechanism of Deep Bolivian Quake

PAGES 9–10

While big earthquakes typically wreack havoc for humankind, the biggest deep earthquake ever recorded—the magnitude 8.3 event that occurred 637 km beneath the surface of Bolivia on June 9, 1994—has brought enlightenment—of sorts.

Instead of bringing death and destruction, the recent Bolivian quake, the largest quake of any type in recent decades, has given scientists one of the best probes yet of the Earth's interior. Within several minutes of the deep rupture, the quake benignly shook the ground from Argentina to Canada. But more important, the quake shook the Earth like a bell for months thereafter, giving scientists a raw data set of the planet's free oscillations—like none other.

The oscillations generated by the Bolivia quake are particularly valuable not only because they are from a big deep quake, but also because they were the first to be captured by a modern-day seismic network. Data from shallow events are not as useful for studying these normal mode vibrations because of the interference caused by surface seismic waves. By analyzing the frequency oscillations from deep events, scientists have been able to determine the density and related properties of rock in various parts of the mantle. Geoscientists need these calculations to decipher the mechanisms that shift the Earth's plates. The Bolivia data set may be the most comprehensive—if not the most heavily scrutinized—yet, according to Steve Kirby of the U.S. Geological Survey in Menlo Park.

Of primary interest is elucidating the mechanism of deep-focus events—the nature of which, both seismologically and physically, has long been controversial. This topic was the focus of almost an entire day of discussion at AGU's Fall Meeting.

Even with the state-of-the-art seismic network, some answers may remain elusive. As Caltech seismologist Hiroo Kanamori puts it: "No matter what you use, there is some limit to the detail [of the seismological mechanism] that can be obtained."

Barriers to Understanding

The main obstacle to learning about the mechanism of deep-focus earthquakes has been that scientists have no direct way to observe the fault zone. In addition, until the Bolivian event, existing seismic and geodetic data had been somewhat limited. The first deep quakes identified by scientists date back to the early 1900s. Prior to that time, scientists generally believed ruptures were not possible at such depths, even though deep quakes exhibit seismic energy patterns that are similar to those of shallow events.

Scientists have generally explained the similarities between the seismic radiation patterns of shallow and deep quakes by a "double couple" source model or various combinations thereof.

Scientists have thought for some time that conventional faults or so-called brittle failure faults cannot form in rock subjected to the conditions found at the depths of the Bolivian quake, which occurred where the Nazca plate is being subducted beneath the mantle of the South American continent. Deep quakes generally occur in areas where subduction is taking place.

At depths of 70 km and above, on the other hand, where surface quakes are found, brittle-failure faulting is exactly what happens. Surface quakes occur in brittle crust that is simultaneously being pushed or pulled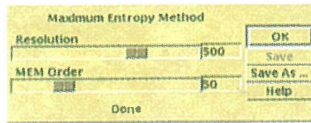 in more than one direction. When the rock eventually breaks, faults form, which in turn can generate quakes, as stress is built up along a given fault and then released.

Mechanisms Explored

Scientists have looked to other mechanisms to explain deep earthquakes from shear instability to delayed deformation. However, the problem has remained that there has been no sure-fire way to test these models. The Bolivia event presents the best shot at it for now.

One of the leading models has been transformational faulting, wherein a phase transition triggers the rupture. However, a large volume change is not thought to be generated because of the ambient shear stress. In this model, the atoms of the mantle rock known as olivine $(Mg,Fe)_2SiO_4$, are somehow rearranged to form a more condensed mineral called spinel, as both the temperature and pressure increase when the descending slab starts to move. Scientists generally believe that the differing strengths of the minerals may account for the sudden slip of the fault, as layers of spinel continue to descend into the Earth.

Perhaps not too surprisingly, reconciling the Bolivia data with the reigning model has not been an entirely straightforward process. Preliminary analyses reveal that the volume change in deep quakes is likely very, very small, while the stress drop is likely to be very large at about 1 kilobar. Yet the rupture velocity is very slow at about 1 km/s, especially with respect to the shear velocity, which is about 6 km/s. In other words, a large fraction of energy was expended for some thing other than radiating seismic waves, Caltech's Kanamori suggests. "Some other process must be involved."

To explain these data, Kanamori and his colleague Masayuki Kikuchi of Yokohama City University in Japan have proposed a new twist to the phase transition model: Melting

Input Signal

Maximum Entropy Spectrum

SSA Eigenvalues

Spectral Analysis Toolkit v 2.2

Input File
SOI

Analysis Tools
FFT Spectrum
Maximum Entropy   Show Log
Multi-Taper Method   QUIT
Singular Spectrum Analysis

Maximum Entropy Method

Resolution   500   OK
                                        Save
MEM Order   50   Save As ...
                                        Help
Done

Singular Spectrum Analysis

Window Length   50
# of Significant Components   8

Variance T-EOFs T-PCs Filtered RCs
Done

Pairing Criteria   Error Bars   Covariance
■ same frequency   ♦ Ghil & Mo   ♦ Burg
☐ strong fft   ∨ Vautard & Ghil ∨ Vautard et al.
☐ do trend test   ∨ inverse lag-one ∨ Broomhead & King

Monte Carlo Test...   OK
                                  Save
                                  Save As ...

Fig. 1.   Toolkit menu and SOI time-series plot, with months from January 1933 on the abscissa and dimensionless SOI values on the ordinate.
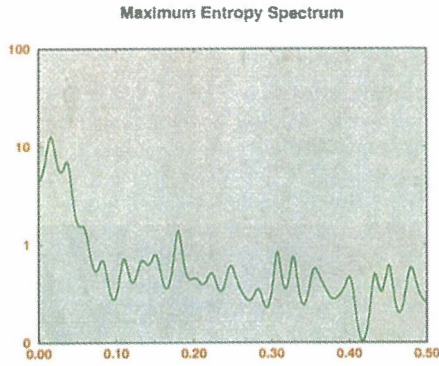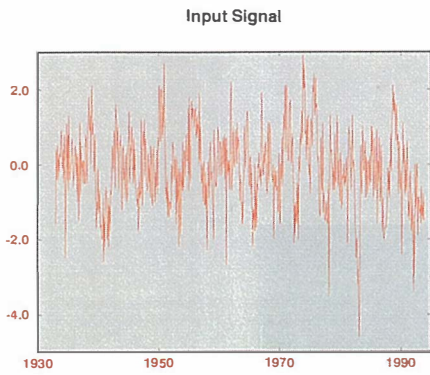
Fig. 2.   MEM menu and MEM power spectrum, with frequency in cycles/month on the abscissa and power in months x (dimensionless SOI)^2 on the ordinate.
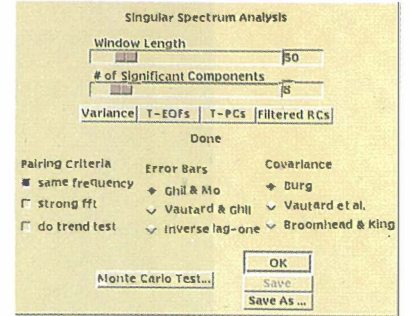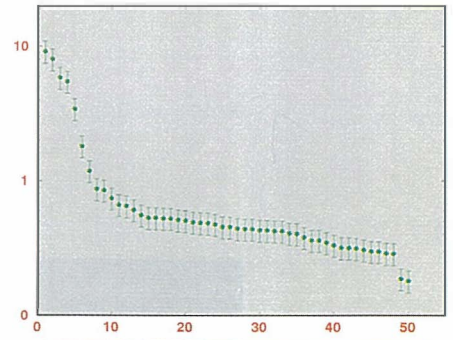
Fig. 3.   SSA menu and log-eigenvalue spectrum for the SOI time series, with SSA component number on the abscissa and percentages of total variance on the ordinate. The components are ordered by variance captured.

Page 12

Reconstructed Components
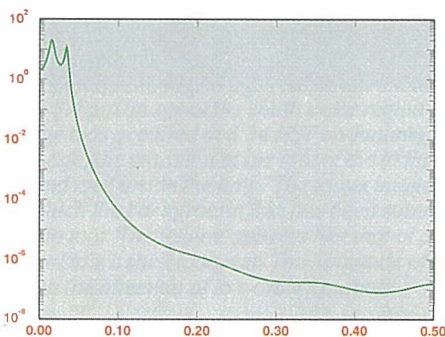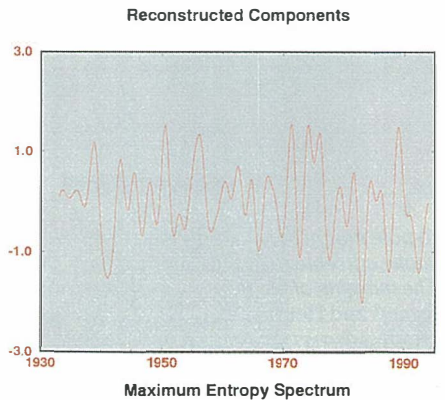
Maximum Entropy Spectrum

Fig. 4.   (a) Reconstruction of SSA components 1-4; same units as in Figure 1b. (b) MEM power spectrum of the SSA-filtered time series shown in (a); same units as in Figure 2.

Page 14